ELSEVIER

Contents lists available at ScienceDirect

Materials Science & Engineering B

journal homepage: www.elsevier.com/locate/mseb





Room temperature polar and weak-ferromagnetic oxide with low dielectric loss

Nagamalleswari Katragadda ^a, Pranab Mandal ^{a,*}, Premakumar Yanda ^b, A. Sundaresan ^b, S.D. Kaushik ^c, Weiguo Zhang ^d, P. Shiv Halasyamani ^d, Alicia María Manjón-Sanz ^e

- ^a Department of Physics, SRM University AP, Amaravati 522240, Andhra Pradesh, India
- b School of Advanced Materials, Chemistry, and Physics of Materials Unit, Jawaharlal Nehru Centre for Advanced Scientific Research, Jakkur P.O., Bangalore 560 064, India
- ^c UGC-DAE Consortium for Scientific Research Mumbai Centre, R-5 Shed, BARC, Mumbai 400085, India
- ^d Department of Chemistry, University of Houston, Houston, TX 77204-5003, United States
- ^e Neutron Scattering Division, Oak Ridge National Laboratory, Oak Ridge, TN 37831-2008, United States

ARTICLE INFO

Keywords: Perovskites Multiferroic Weak ferromagnetic Polar Impedance spectroscopy

ABSTRACT

Single-phase materials that are simultaneously ferroelectric and ferromagnetic at room temperature are promising for devices such as non-volatile random-access memory. Perovskite BiFeO $_3$ which crystallizes in the polar rhombohedral structure (R3c) is ferroelectric and antiferromagnetic at room temperature. Here, we report a family of perovskite oxides in the BiFeO $_3$ – Bi $_2/_3$ TiO $_3$ – ATiO $_3$ (where A^{2+} is divalent alkaline earth metal ions e. g, Ca $^{2+}$, Sr $^{2+}$, Ba $^{2+}$) ternary phase diagram that is polar as well as weak ferromagnetic above room temperature. The composition (Bi $_0.9167A_0.075$)(Fe $_0.9$ Ti $_0.1$)O $_3$ crystallizes in the polar rhombohedral structure space group R3c as corroborated by powder X-ray and neutron diffraction analysis. The nearly pure A-site perovskite possesses a long-range magnetic ordering above room temperature. These perovskites show a low dielectric loss, and the electrical response is dominated by grain contributions below 723 K.

1. Introduction

Bismuth-based perovskite oxides (BiMO₃, where M³⁺ is a transition metal ion) are promising due to their versatile properties such as Pb-free piezoelectrics, multiferroics, solar cells etc [1–5]. Especially pure A-site bismuth-based perovskite oxides that possess a polar structure are candidates for Pb-free piezoceramics. Among these, only a few perovskites, e.g., BiFeO3, BiTi $_{3/8}$ Fe $_{2/8}$ Mg $_{3/8}$ O3, are accessible at ambient pressure [6,7] whereas BiMnO₃, BiInO₃, BiNiO₃, and BiAlO₃ are high-pressure phases [8-10]. BiFeO₃ has been extensively studied as a candidate material for room-temperature multiferroic [3,11–13], and piezoceramics [2,14] and has been demonstrated in random access memory device applications. At room temperature, the structure of BiFeO3 is rhombohedral (space group R3c) with ferroelectric polarization along the [111]_p direction. Ferroelectric switching has been reported in both ceramics and thin-film heterostructures with polarization as high as 60 μ C/cm² [13,15]. The long-range G-type magnetic ordering in BiFeO₃ onsets below 675 K, however, the magnetic structure is modulated with a cycloidal ordering with a long period of 620 Å along the [110]h

direction [16]. This modulation cancels any net magnetization due to Dzyaloshinsky-Moriya interaction as commonly observed in rare-earth orthoferrites. Epitaxial strain, chemical substitution at the A-site or Bsite by Ti, and pressure has been shown to improve the magnetization in BiFeO₃ [12,14,17–24]. For example, the polar and weak ferromagnetic phase is sustained up to $x\,=0.11$ in $BiFe_{1\text{-}x}Ti_xO_{3+\delta}$ and up to $x\,=0.2$ in $Bi_{1-x}A_xFeO_3$ where A = La, Ca, Sr, Ba) [25–27]. New design routes can lead to materials that are both ferroelectric and ferromagnetic above room temperature. For example, a bulk perovskite oxide exhibited both switchable polarization and magnetization from a design strategy that led to improved ferroelectric properties at the morphotropic phase boundary and a sustained long-range magnetic order from a percolating network of magnetic ions [28,29]. Synthesis and ceramic processing of BiFeO₃ are known to be challenging due to its phase instability, competing secondary phases, bismuth volatility, and purity of starting oxides and precautions are necessary to overcome these challenges [11,30,31].

Rare earth orthoferrites, e.g., LaFeO₃, have a perovskite structure where trivalent La and Fe occupy the A and B sites of the perovskite,

E-mail address: pranab.m@srmap.edu.in (P. Mandal).

^{*} Corresponding author.

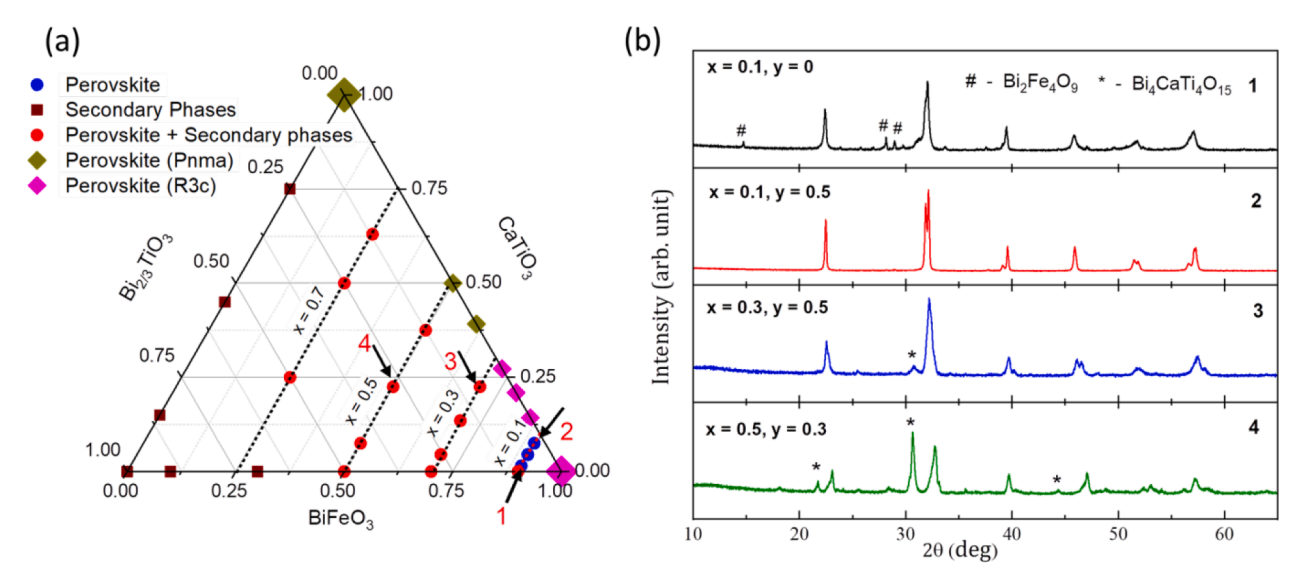


Fig. 1. (a) Ternary phase diagram of BiFeO₃ – Bi_{2/3}TiO₃ – ATiO₃ for $A^{2+} = Ca^{2+}$. Filled blue circles represent phase pure perovskite phase (this study), filled red circles represent perovskite with secondary phases (this study), filled brown squares represent secondary phases (this study), and magenta and olive squares represent BiFeO₃ – CaTiO₃. (b) Selected XRD pattern of (1-x)BiFeO₃ – xBi_{2/3-y}A_{3y/2}TiO₃ for $A^{2+} = Ca^{2+}$. The secondary phases Bi₂Fe₄O₉ and Bi₄CaTi₄O₁₅ are marked by the symbols # and *. Unindexed peaks represent the perovskite phase. (For interpretation of the references to colour in this figure legend, the reader is referred to the web version of this article.)

respectively [32]. There are only a few A-site deficient perovskites known in the literature, *e.g.*, $La_{2/3}TiO_{3}$, which accommodates cations of higher oxidation states at the B-site [33,34]. It has been reported that the bismuth analog of $La_{2/3}TiO_{3}$, *i.e.*, $Bi_{2/3}TiO_{3}$ [35], aids to improve the density and resistivity of PbTiO₃ ceramics [36]. Here, we have studied the effect of $Bi_{2/3}TiO_{3}$ substitution on the ferroelectric and magnetic properties of $BiFeO_{3}$. The $BiFeO_{3}$ – $Bi_{2/3}TiO_{3}$ solid solution avoids Bi^{3+} dilution at the A-site and introduces Ti^{4+} at the B-site. The lone pair effect of Bi^{3+} at the A-site and second order Jahn-Teller effect due to the closed-shell (d^{0}) electronic configuration of Ti^{4+} ion is expected to promote ferroelectricity in these perovskites [37]. We find that the stability of the perovskite phase improves in the $BiFeO_{3}$ – $Bi_{2/3}TiO_{3}$ – $ATiO_{3}$ ternary phase diagram where $A^{2+} = Ca^{2+}$, Sr^{2+} , and Ba^{2+} . The resulting perovskite oxides are simultaneously polar and weak ferromagnetic at room temperature with about 90% bismuth at the A-site.

2. Materials and methods

The compounds in the BiFeO₃ – Bi_{2/3}TiO₃ – ATiO₃ (A^{2+} = Ca²⁺, Sr²⁺, Ba²⁺) were prepared by conventional solid-state route using high-purity starting materials; Bi₂O₃ (>99 % Loba Chemie), CaCO₃ (>99 % Loba Chemie), SrCO₃ (>99 % Loba Chemie), BaCO₃ (>99 % Loba Chemie), TiO₂ (>99 % Loba Chemie), and Fe₂O₃ (>95 % Loba Chemie). The details of the compositions prepared in this study are summarized in Tables S1 and S2, Supporting information. The starting materials were preheated at 180 °C for 10 h to remove any moisture. The stoichiometric ratio of starting oxides and carbonates was mixed in an agate mortar pestle in acetone. The homogenized powders were calcined in an alumina crucible at 750 °C, 800 °C, and 850 °C for 12 h with intermittent grindings between heating. The phase pure powders were mixed with a binder (Polyvinyl butyral 2 wt%), pressed into pellets, and sintered at temperatures between 870 and 950 °C to obtain pellets above 90% of the crystallographic density. The phase purity and crystal structure were studied using powder X-ray diffraction (XRD) using CuK- α radiation in a powder X-ray diffractometer (PANalytical Empyrean). Powder neutron diffraction (PND) experiments were carried out employing POWGEN diffractometer (Spallation Neutron Source at Oak Ridge National Laboratory) [38] and PD3 multi PSD based focusing crystal diffractometer set up by UGC-DAE Consortium for Scientific Research Mumbai Centre at the National Facility for Neutron Beam Research (NFNBR), Dhruva

reactor, Mumbai, India [39]. For the experiment at POWGEN, around 3 g of sample was placed in a 6 mm diameter vanadium can and loaded into the vacuum furnace. The data were collected at 300 K for 2 h. A central wavelength of 1.5 Å was used, covering a d-spacing of 0.5-10.85 Å. Structural analysis was carried out using software packages High-Score (XRD data), Fullprof [40] (BARC data), and TOPAS-Academic POWGEN data) [41]. Microstructure and composition were studied using a Hi-Resolution Scanning Electron Microscope (HRSEM) (Thermosceintific Apreo S). For dielectric and ferroelectric measurements. polished pellets of thickness 150–200 µm were painted with silver paste and cured at 120 °C for 1 h. An LCR meter E4980A was utilized to evaluate dielectric properties in the frequency range between 100 Hz and 1 MHz. Complex impedance properties were measured using a custom-made furnace and impedance probe setup [42]. The ferroelectric hysteresis loops were evaluated at room temperature by a Precision Multiferroic II Ferroelectric Test System (Radiant Technologies, Inc., USA). The Second harmonic generation (SHG) was measured by using a 1064 nm pulsed Nd: YAG laser (Quantel Laser, Ultra 50) to offer the fundamental light and the generated second harmonic light to be detected and monitored by an oscilloscope system (Tektronix, TDS3032). Samples were filled in fused silica tubes with an outer diameter of 4 mm. Relevant comparisons with known SHG material, α-SiO₂, were made at the same condition. The laser-generated fundamental light and the SHG intensity were recorded at room temperature on an oscilloscope [43]. The DC magnetization data was collected in zero-field-cooled (ZFC) and field-cooled (FC) modes using a magnetic property measurement system (MPMS, Quantum Design, USA). For high-temperature magnetic data, the measurements were carried out in an oven option of the Physical property measurement system (PPMS, Quantum Design, USA).

3. Results and discussion

3.1. Materials synthesis

Attempt to synthesize Bi $_{2/3}$ TiO $_3$ at 850 °C for 12 h resulted in various secondary phases (Bi $_4$ Ti $_3$ O $_{12}$, Bi $_8$ Ti $_1$ 6O $_4$ 4), and there was no indication of the perovskite phase (Fig. S1, Supporting Information). It should be noted that Bi-based perovskite e.g., BiMnO $_3$, BiCrO $_3$, BiAlO $_3$, and BiInO $_3$ are metastable phases that can only be stabilized by high-pressure

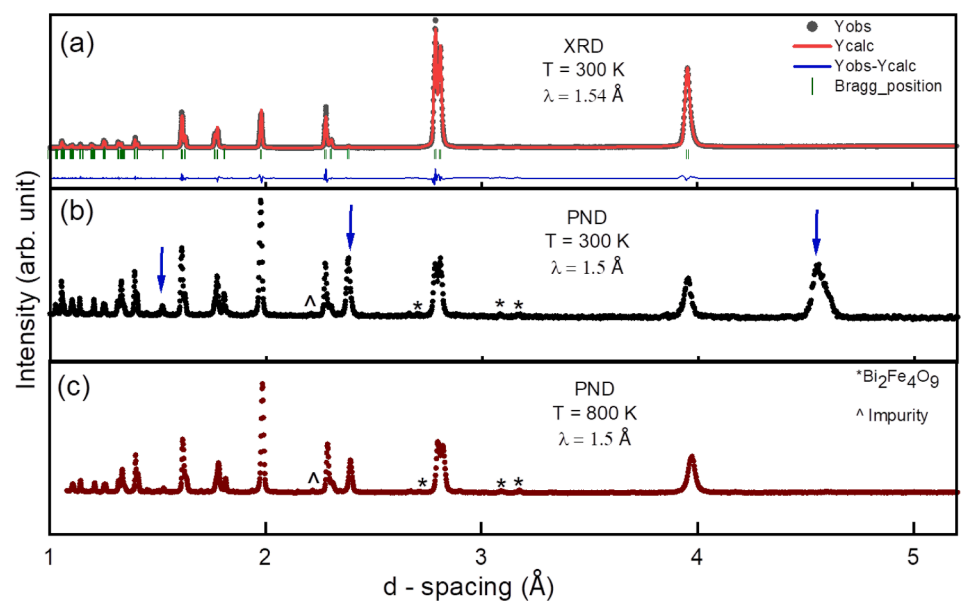


Fig. 2. (a) Profile fit to room-temperature powder X-ray diffraction data of BCFT15. Black points show the data, Red lines the fit, blue line the difference plot, and green markers show Bragg positions (b) A strong reflection near d $\sim 4.56~\mbox{\normale}A$ in 300 K PND data (POWGEN) confirms longrange magnetic ordering; the blue arrow indicates the magnetic peaks (c) PND data at 800 K (POWGEN) showing absence magnetic peak consistent with magnetization data (Fig. 3). Small amount of secondary phases indicated with * and^represents Bi_2Fe_4O_9 and unidentified impurity respectively. (For interpretation of the references to colour in this figure legend, the reader is referred to the web version of this article.)

synthesis. It is possible that $Bi_{2/3}TiO_3$ could be a metastable phase and cannot be stabilized using the ambient pressure solid state route. Divalent alkaline earth metal ions ($A^{2+} = Ca^{2+}$, Sr^{2+} , Ba^{2+}) were substituted at the Bi-site to stabilize $Bi_{2/3}TiO_3$ in the perovskite phase in the range $0.1 \le y \le 0.5$ in $Bi_{2/3-y}A_{3y/2}TiO_3$. The calculated tolerance factor $Bi_{2/3-y}Ca_{3y/2}TiO_3$ is near the perovskite limit (0.95 – 1.05) as shown in Table S1 (Supporting Information). The XRD patterns indicate secondary phases (Fig. S1, Supporting Information). These compositions are shown in the $Bi_{2/3}TiO_3$ – $CaTiO_3$ line in the ternary phase diagram Fig. 1a.

We then prepared $(1-x)BiFeO_3-xBi_{2/3}TiO_3$ using the solid-state route. Powder XRD patterns show that the compositions x=0.9 and 0.7 were formed with secondary phases, with no indication of a perovskite phase (Fig. S2, Supporting Information). This is indicated as the brown squares in the $Bi_{2/3}TiO_3 - BiFeO_3$ line (baseline of the triangle) in the ternary phase diagram (Fig. 1a). For x=0.5 and 0.3, a perovskite phase forms with other secondary phases as represented using filled red circles in the ternary phase diagram. The calculated tolerance factor of compositions in (1-x) $BiFeO_3-xBi_{2/3}TiO_3$ ranges from t=0.84 to t=0.84

0.95 for x = 0.7 to x = 0.1, respectively.

To tune the tolerance factor towards the perovskite range (\sim 0.94 to 1.04), divalent alkaline earth metal ions were substituted at the Bi-site in the solid solution $(1-x)BiFeO_3 - xBi_{2/3-y}A_{3y/2}TiO_3$ $(A^{2+} = Ca^{2+}, Sr^{2+},$ Ba²⁺) which can be represented in the ternary phase diagram of BiFeO₃ – $Bi_{2/3}TiO_3$ - $ATiO_3$ (A^{2+} = Ca^{2+} shown in Fig. 1a). As can be seen from Fig. 1b, the introduction of divalent Ca²⁺ has a significant effect on the phase purity. For x = 0.3, y = 0.1-0.5 (x = 0.3 dotted line), and x = 0.5, y = 0.1-0.5 (x = 0.5 dotted line) the phase purity improves; however, the perovskite phase forms with other impurities represented filled by red circles. For x = 0.1, y = 0.3, and x = 0.1, y = 0.5 phase pure perovskite forms as indicated by filled blue circles (x = 0.1, y = 0.5shown as pattern 2 in Fig. 1b). Ternary phase diagrams with $A^{2+} = Sr^{2+}$ and Ba²⁺ show similar trends as shown in Table S2 (Supporting Information). The compositions in the solid solution (1-x)BiFeO $_3$ - xBi $_2/$ $_{3-y}A_{3y/2}$ TiO₃ for $A^{2+} = Ca^{2+}$, Sr^{2+} , and Ba^{2+} are represented as BCFTxy, BSFTxy, and BBFTxy respectively as summarized in Table S1 and Table S2, Supporting Information. In this work, BCFT15 (x = 0.1, y = 0.5for $A^{2+} = Ca^{2+}$) and BSFT15 (x = 0.1, y = 0.5 for $A^{2+} = Sr^{2+}$) have been

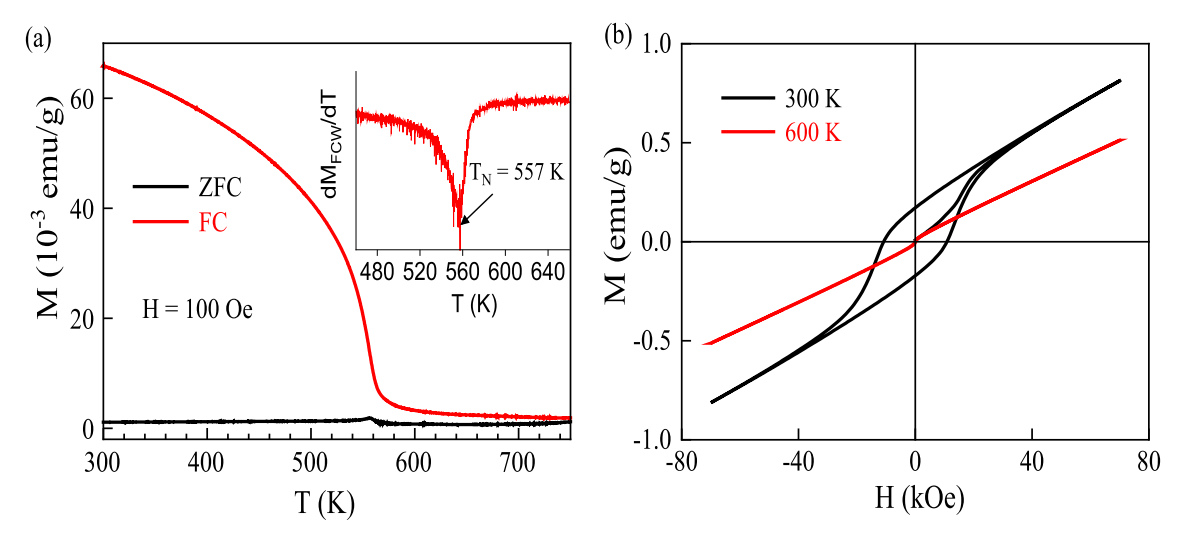


Fig. 3. (a) Zero-field cooled (ZFC) and field cooled (FC) magnetization data of BCFT15 against temperature showing magnetic ordering at 557 K as calculated from the derivative of FC data (inset). (b) Magnetic isotherm at 300 K (black line) and 600 K (red line) of composition BCFT15 confirmed weak ferromagnetism at room temperature. (For interpretation of the references to colour in this figure legend, the reader is referred to the web version of this article.)

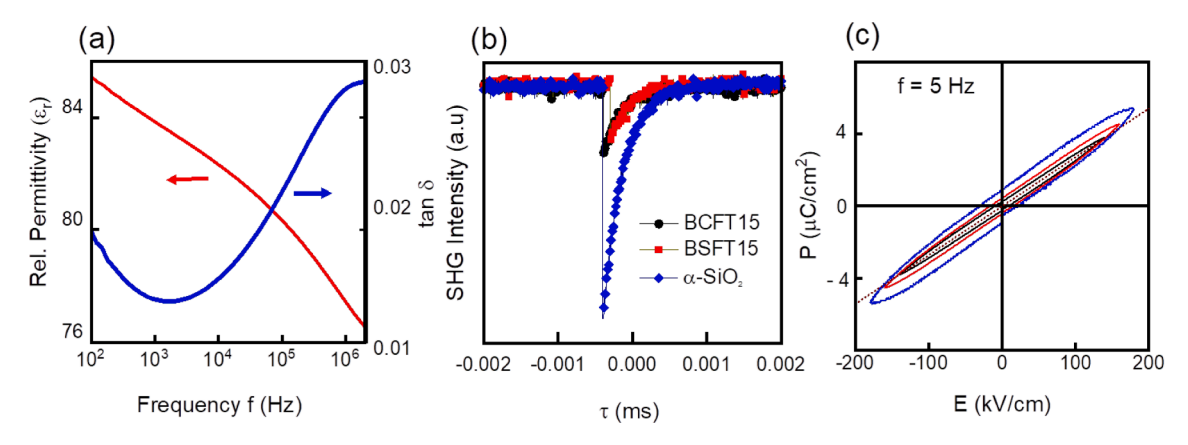


Fig. 4. (a) Room-temperature dielectric constant (left axis) and dielectric loss (right axis) plotted against frequency for BCFT15, (b) Second harmonic generation measurement at room temperature on BCFT15 and BSFT15, (c) Room temperature polarization – electric field (P(E)) loops of BCFT15 measured at increasing field values at a frequency of 5 Hz.

studied in detail.

3.2. Structural analysis

Structural analysis was focused on the phase pure perovskite composition BCFT15. Profile fit to the laboratory X-ray data on BCFT15 confirms that all the reflections can be explained by the rhombohedral space group R3c. A small amount (<2 %) of secondary phases was present (Fig. 2). The refined lattice parameters obtained from the profile fit are a = 5.5670 (2) Å, c = 13.8034(2) Å and V = 370.47 Å³. The change in lattice parameters from the lattice parameters of BiFeO₃ (a = 5.579 Å, c = 13.869 Å, and V = 373.44 Å³) suggests that a solid solution is formed. Preliminary Rietveld refinement suggests a reasonably fit to space group R3c and the structural parameters are provided in Fig. S4 and Table S3, Supporting Information. The reduction in cell parameters is due to the difference in the ionic radii of Bi³⁺ (r = 1.17 Å), Ca²⁺ (r =1.34 Å), Fe^{3+} (r = 0.645 Å), and Ti^{4+} (r = 0.605 Å) [7,31]. A similar trend has been observed in the solid solution of BiFeO₃ and CaTiO₃ [30]. It is noteworthy, that in BiFeO₃ - CaTiO₃, the polar rhombohedral structure (R3c) of BiFeO₃ extends up to x = 0.2, and above the limit, the structure changes to a non-polar orthorhombic structure with space group Pnma [44]. The powder XRD patterns of compositions BAFT11 and BAFT13 for $A^{2+} = Ca^{2+}$, Sr^{2+} , and Ba^{2+} show a similar trend, and the patterns can be explained using the rhombohedral structure R3c (Table S2, Supporting Information). Second harmonic generation (SHG) experiments were conducted on compositions BAFT13, BAFT15 for A^{2+} = Ca²⁺, Sr²⁺, and Ba²⁺. All six compositions are found to be SHG active and corroborate with the polar or non-centrosymmetric structure [43,45] (data shown in Fig. 4b for BCFT15 and BSFT15). The SHG data for other compositions are shown in (Fig. S6 Supporting Information). The SEM micrographs of the composition BCFT15, and BSFT15 show a typical grain-like feature with an average microparticle size of 1-2 μm (Fig. S3, Supporting Information). The average compositions were calculated from energy-dispersive X-ray spectroscopy (EDX) measurements for BCFT15 and BSFT15 are (Bi_{0.804}Ca_{0.061})(Fe_{0.9}Ti_{0.099})O₃ and (Bi_{0.740}Sr_{0.059})(Fe_{0.9}Ti_{0.077})O₃ which are close to their target compositions $(Bi_{0.9167}Ca_{0.075})(Fe_{0.9}Ti_{0.1})O_3$ and $(Bi_{0.9167}Sr_{0.075})(Fe_{0.9}Ti_{0.1})O_3$ respectively. The profile fit, lattice parameter trend, and compositional analysis exclude the possibility of phase separation and therefore the SHG response is consistent with the polar structure with space group R3c.

The room temperature PND data of BCFT15 (Fig. 2b) reveals a strong reflection at d \sim 4.56 Å. This reflection is not allowed in the rhombohedral space group $\it R3c$ and is absent in the XRD data (Fig. 2a). This suggests the possibility of long-range magnetic ordering which was further corroborated by the subsequent magnetization measurement.

The reflection at 4.56 Å in PND data disappears at high temperatures which is consistent with magnetic measurements (Fig. 2c and Fig. 3a). Preliminary magnetic structure analysis suggests a G-type antiferromagnetic ordering with magnetic moments predominantly aligned in the a-b plane (Fig. S4b, Supporting Information). The refined magnetic moment is $3.07 \, \mu_B$ and matches closely with the existing reports in BiFe_{1. x}Ti_xO₃ and Bi_{1-x}Sr_xFeO₃ [23,25].

3.3. Magnetic properties

Magnetization data collected on BCFT15 in the temperature range of 2 to 400 K show that Zero-field cooled (ZFC) and Field cooled (FC) curves diverge from 400 K and remain down to 2 K (Fig. S5, Supporting Information). No magnetic anomalies were observed in this temperature range, therefore, excluding any spin-reorientation transition as observed in BiFeO₃ at 140 K and 200 K. Further magnetization isotherms collected at room temperature show a magnetic hysteresis loop. The presence of ZFC - FC divergence and magnetic hysteresis loop confirms weak ferromagnetism or canted antiferromagnetic behavior as commonly observed in rare-earth orthoferrites LnFeO3 due to spin-canting. To determine the magnetic ordering temperature, ZFC and FC magnetization were measured in the oven option of the Physical property measurement system PPMS. As shown in Fig. 3a, the sharp onset of FC magnetization and large divergence in ZFC – FC data confirm a magnetic ordering. This is also consistent with the nearly linear magnetic hysteresis loop at 600 K (Fig. 3b). It may be noticed that the small hysteresis at 600 K and slight divergence in ZFC - FC data above T_N may indicate a small amount of magnetic secondary phases which could not be identified using laboratory X-ray data. In particular, the presence of magnetic secondary phases in BiFeO₃-related materials is a complex problem and depends on various other factors such as purity of starting materials, Bi-loss, phase homogeneity, etc [28,31]. The onset of the magnetic ordering as determined from the derivative of FC data is $T_N = 557$ K. The remanent magnetization (M_r) at 300 K is estimated from the M-H isotherm to be 0.01 $\mu_B/f.u.$ The appearance of weak ferromagnetism in BCFT15 can be understood as follows. Unlike in rare earth orthoferrites, the net magnetization caused by antisymmetric Dzyaloshinsky-Moriya interaction is zero due to the incommensurately modulated spin structure below $T_N = 643 \text{ K} [46,47]$. Substitution of nonmagnetic Ti^{4+} in the Fe³⁺ site and Ca²⁺ in the Bi³⁺ site perturbs the spatial spin structure and this, in turn, induces canted antiferromagnetic behavior as observed in orthoferrites and BiFeO₃ – CaTiO₃ [25,44,48].

3.4. Dielectric, and ferroelectric properties

The room temperature dielectric constant in BCFT15 varies from 86

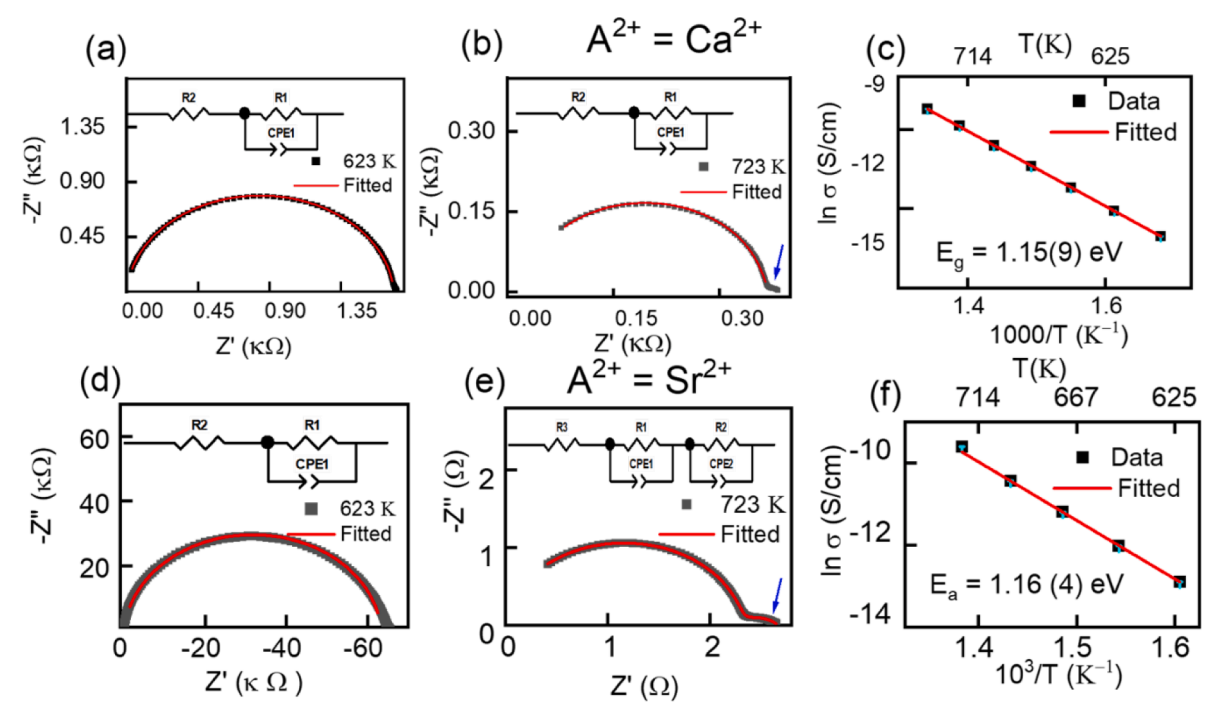


Fig. 5. The Nyquist plots of composition (a, b) for BCFT15 and (d, e) for BSFT15 and Arrhenius fit (c) for BCFT15 and (f) for BSFT15 to the grain conductivity of compositions.

to 77 in the frequency range of 100 Hz to 1 MHz. Interestingly the dielectric loss is low and ranges from 0.01 to 0.03 in the same frequency range (Fig. 4a). It should be noted that the processing of BiFeO $_3$ and related ceramic oxides is challenging, and high dielectric loss can result in artifacts in ferroelectric measurements. The loss data presented here is similar to the reported values in BiFeO $_3$ – CaTiO $_3$ system [44]. The low loss in these oxides facilitated measurements up to 180 kV/cm during ferroelectric polarization versus electric field (P(E)) loop measurements. As the external field increases, the polarization data evolves in a nonlinear way (Fig. 4c) indicating domain wall motion [27,49]. It should be cautioned that the loops presented here do not demonstrate ferroelectricity and may require the application of a higher electric field for polarization switching.

3.5. Complex impedance study

To understand the origin of the dielectric behavior, the complex impedance spectroscopy (CIS) technique was employed. Fig. 5a, b and Fig. 5d, e shows the complex impedance spectra (Nyquist plot) at selected temperatures for BCFT15 and BSFT15 respectively. The impedance plots at lower temperatures can be explained in terms of a single contribution arising from grains. The data has been modeled using a parallel circuit consisting of resistance (R) and a constant phase element CPE $(Y_{CPE} = \frac{1}{Z_{CPE}} = A_0 (j\omega)^n)$ where A_0 and n are constants for a given temperature (0 $\leq n \leq$ 1). The equivalent capacitance (C = $R^{\frac{1-n}{n}}$ $Q_n^{\frac{1}{n}}$) is of the order of 10^{-11} F suggesting a contribution from the grains [50]. The activation energy (Ea) is obtained from the grain conductivity (σ_{dc}) vs $10^3/T$ plot using Arrhenius equation $(\sigma_{dc} = \sigma_0 e^{-\frac{E_a}{k_B T}})$ [51]. The activation energy obtained from the linear fit is 1.15(9) eV and 1.16(4) eV respectively for BCFT15 and BSFT15 compositions (Fig. 5c, f). The compositions show predominantly grain contribution between 500 K and 623 K whereas above 650 K an additional arc appears in the impedance plots as shown by blue arrows (Fig. 5b, e). The equivalent capacitance is found to be of the order of 10⁻⁶ F indicating electrode contribution [24,50].

4. Conclusions

We explored $BiFeO_3 - Bi_{2/3}TiO_3 - ATiO_3$ where $(A^{2+} = Ca^{2+}, Sr^{2+}, Ba^{2+})$ ternary phase diagram and achieved perovskite phases with high-bismuth content at the A-site. Preliminary Rietveld measurements suggest a polar rhombohedral structure (Space group R3c) akin to the parent $BiFeO_3$. These compositions show a low dielectric loss, and the electrical response is dominated by grain contribution. PND and DC magnetic measurements confirm long-range magnetic ordering below 557 K. At room temperature, these compositions are both polar and weak ferromagnetic. The strategy would be helpful to design new room-temperature polar magnetic materials.

Declaration of Competing Interest

The authors declare that they have no known competing financial interests or personal relationships that could have appeared to influence the work reported in this paper.

Data availability

Data will be made available on request.

Acknowledgments

Dr. P. Mandal and Ms. K N Malleswari acknowledge the financial support of the Early Career Research Grant from the Science and Engineering Research Board (SERB), India Grant No. ECR/2018/001252. The authors acknowledge the financial support from UGC-DAE CSR, India through a Collaborative Research Scheme (CRS) project number CRS/2021-22/03/562. A portion of this research used resources at the Spallation Neutron Source, a DOE Office of Science User Facility operated by the Oak Ridge National Laboratory (IPTS-26971). WZ and PSH thank the Welch Foundation (Grant E-1457) and the NSF (DMR-2002319) for their support.

Appendix A. Supplementary data

Supplementary data to this article can be found online at https://doi.org/10.1016/j.mseb.2023.116869.

References

- [1] G. Chen, J. Chen, W. Pei, Y. Lu, Q. Zhang, Q. Zhang, Y. He, Bismuth ferrite materials for solar cells: current status and prospects, Mater. Res. Bull. 110 (2019) 39–49, https://doi.org/10.1016/j.materresbull.2018.10.011.
- [2] J. Wu, Perovskite lead-free piezoelectric ceramics, J. Appl. Phys. 127 (2020), 190901, https://doi.org/10.1063/5.0006261.
- [3] N.A. Spaldin, R. Ramesh, Advances in magnetoelectric multiferroics, Nat. Mater. 18 (2019) 203–212, https://doi.org/10.1038/s41563-018-0275-2.
- [4] S. Kossar, R. Amiruddin, A. Rasool, M.S. Kumar, N. Katragadda, P. Mandal, N. Ahmed, Study on ferroelectric polarization induced resistive switching characteristics of neodymium-doped bismuth ferrite thin films for random access memory applications, Curr. Appl. Phys. 39 (2022) 221–229, https://doi.org/ 10.1016/j.cap.2022.04.013.
- [5] M. Kumar, P.C. Sati, A. Kumar, M. Sahni, P. Negi, H. Singh, S. Chauhan, S. K. Chaurasia, Recent advances on magnetoelectric coupling in BiFeO₃: technological achievements and challenges, Mater. Today.. Proc. 49 (2022) 3046–3049, https://doi.org/10.1016/j.matpr.2020.10.685.
- [6] C.A. Bridges, M. Allix, M.R. Suchomel, X. Kuang, I. Sterianou, D.C. Sinclair, M. J. Rosseinsky, A pure bismuth a site polar perovskite synthesized at ambient pressure, Angew. Chem. Int. Ed. 46 (2007) 8785–8789, https://doi.org/10.1002/anie.200703146.
- [7] R.D. Shannon, Revised effective ionic radii and systematic studies of interatomic distances in halides and chalcogenides, Acta Cryst. A 32 (1976) 751–767, https:// doi.org/10.1107/S0567739476001551.
- [8] A.A. Belik, T. Wuernisha, T. Kamiyama, K. Mori, M. Maie, T. Nagai, Y. Matsui, E. Takayama-Muromachi, High-pressure synthesis, crystal structures, and properties of perovskite-like BiAlO3 and pyroxene-like BiGaO₃, Chem. Mater. 18 (2006) 133–139, https://doi.org/10.1021/cm052020b.
- [9] A.A. Belik, S.Y. Stefanovich, B.I. Lazoryak, E. Takayama-Muromachi, BiInO₃: a polar oxide with GdFeO₃-type perovskite structure, Chem. Mater. 18 (2006) 1964–1968, https://doi.org/10.1021/cm052627s.
- [10] A. Sundaresan, R. Mangalam, A. Iyo, Y. Tanaka, C. Rao, Crucial role of oxygen stoichiometry in determining the structure and properties of BiMnO₃, J. Mater. Chem. A 18 (2008) 2191. https://doi.org/10.1039/B803118P.
- [11] S. Hao, J. Yi, X. Chao, L. Wei, Z. Yang, Multiferroic properties in Mn-modified 0.7BiFeO₃ 0.3(Ba_{0.85}Ca_{0.15})(Zr_{0.1}Ti_{0.9})O₃ ceramics, Mater. Res. Bull. 84 (2016) 25–31, https://doi.org/10.1016/j.materresbull.2016.07.012.
 [12] J. Wang, J. Neaton, H. Zheng, V. Nagarajan, S. Ogale, B. Liu, D. Viehland,
- [12] J. Wang, J. Neaton, H. Zheng, V. Nagarajan, S. Ogale, B. Liu, D. Viehland, V. Vaithyanathan, D. Schlom, U. Waghmare, Epitaxial BiFeO3 multiferroic thin film heterostructures, Science 299 (2003) 1719–1722, https://doi.org/10.1126/ science.1080615.
- [13] S.O. Leontsev, R.E. Eitel, Progress in engineering high strain lead-free piezoelectric ceramics, Sci. Technol. Adv. Mater. 123 (11) (2010) 044302, https://doi.org/ 10.1088/1468-6996/11/4/044302.
- [14] J. Wei, High-temperature ferroic phase transitions and paraelectric cubic phase in multiferroic Bi_{0.95}+δFe_{0.9}Zr_{0.1}O₃, Appl. Phys. Lett. 96 (2010) 114106, https://doi. org/10.1063/1.4729484
- [15] F. Chen, Q. Zhang, J. Li, Y. Qi, C. Lu, X. Chen, X. Ren, Y. Zhao, Sol-gel derived multiferroic BiFeO₃ ceramics with large polarization and weak ferromagnetism, Appl. Phys. Lett. 89 (2006), 092910, https://doi.org/10.1063/1.2345603.
- [16] G. Smolenskiĭ, I. Chupis, Ferroelectromagnets, Sov. phys., Usp. 25 (1982) 475. https://iopscience.iop.org/article/10.1070/PU1982v025n07ABEH004570.
- [17] G. Yuan, S.W. Or, Multiferroicity in polarized single-phase Bi_{0.875}Sm_{0.125} FeO₃ ceramics, J. Appl. Phys. 100 (2006), 024109, https://doi.org/10.1063/1.2220642.
- [18] S. Zhang, L. Wang, Y. Chen, D. Wang, Y. Yao, Y. Ma, Observation of room temperature saturated ferroelectric polarization in Dy substituted BiFeO₃ ceramics, L. Appl. Phys. 111 (2012), 074105, https://doi.org/10.1063/1.3702405.
- J. Appl. Phys. 111 (2012), 074105, https://doi.org/10.1063/1.3702405.
 S.-T. Zhang, Y. Zhang, M.-H. Lu, C.-L. Du, Y.-F. Chen, Z.-G. Liu, Y.-Y. Zhu, N.-B. Ming, X. Pan, Substitution-induced phase transition and enhanced multiferroic properties of Bi_{1-x}La_xFeO₃ ceramics, Appl. Phys. Lett. 88 (2006), 162901, https://doi.org/10.1063/1.2195927.
- [20] V. Khomchenko, D. Kiselev, J. Vieira, L. Jian, A. Kholkin, A. Lopes, Y. Pogorelov, J. Araujo, M. Maglione, Effect of diamagnetic Ca, Sr, Pb, and Ba substitution on the crystal structure and multiferroic properties of the BiFeO₃ perovskite, J. Appl. Phys. 103 (2008), 024105, https://doi.org/10.1063/1.2836802.
- [21] Y.F. Popov, A. Zvezdin, Magnetoelectric effect and toroidal ordering in Ga_{2-x}Fe_xO₃, JETP Lett. 57 (1993) 146–151, https://doi.org/10.1134/1.5586
- [22] I. Sosnowska, T.P. Neumaier, E. Steichele, Spiral magnetic ordering in bismuth ferrite, J. Phys. C Solid State Phys. 15 (1982) 4835. https://iopscience.iop.org/art icle/10.1088/0022-3719/15/23/020.
- [23] I. Troyanchuk, M. Bushinsky, D. Karpinsky, V. Sirenko, V. Sikolenko, V. Efimov, Structural and magnetic phases of $Bi_{1-x}A_xFeO_{3-\delta}(A=Sr,Pb)$ perovskites, Eur. Phys. J. B 73 (2010) 375–381, https://doi.org/10.1140/epjb/e2010-00004-y.
- [24] M. Rangi, A. Agarwal, S. Sanghi, R. Singh, S. Meena, A. Das, Crystal structure and magnetic properties of Bi_{0.8}A_{0.2}FeO₃ (A = La, Ca, Sr, Ba) multiferroics using neutron diffraction and Mossbauer spectroscopy, AIP Adv. 4 (2014), 087121, https://doi.org/10.1063/1.4893241.

- [25] V. Khomchenko, I. Troyanchuk, V. Sikolenko, J. Paixão, Weak ferromagnetic polar phase in the BiFe_{1-x}Ti_xO₃ multiferroics, J. Mater. Sci. 48 (2013) 3852–3856, https://doi.org/10.1007/s10853-013-7186-z.
- [26] H. Dixit, J. Hee Lee, J. Krogel, Stabilization of weak ferromagnetism by strong magnetic response to epitaxial strain in multiferroic BiFeO₃, Sci. Rep. 5 (2015) 12969, https://doi.org/10.1038/srep12969.
- [27] Z. Tylczyński, A collection of 505 papers on false or unconfirmed ferroelectric properties in single crystals, ceramics and polymers, Front. Phys. 14 (2019) 63301, https://doi.org/10.1007/s11467-019-0925-0.
- [28] P. Mandal, M.J. Pitcher, J. Alaria, H. Niu, M. Zanella, J.B. Claridge, M. J. Rosseinsky, Controlling phase assemblage in a complex multi-cation system: phase-pure room temperature multiferroic (1-x) BiTi_{(1-y)/2}FeyMg_{(1-y)/2}O_{3-x}CaTiO₃, Adv. Funct. Mater. 26 (2016) 2523–2531, https://doi.org/10.1002/adfm.201504911.
- [29] P. Mandal, M. Pitcher, J. Alaria, H. Niu, P. Borisov, P. Stamenov, J. Claridge, M. Rosseinsky, Designing switchable polarization and magnetization at room temperature in an oxide, Nature 525 (2015) 363–366, https://doi.org/10.1038/ nature14881
- [30] M. Valant, A.-K. Axelsson, N. Alford, Peculiarities of a solid-state synthesis of multiferroic polycrystalline BiFeO₃, Chem. Mater. 19 (2007) 5431–5436, https://doi.org/10.1021/cm071730+.
- [31] G. Catalan, J.F. Scott, Physics and applications of bismuth ferrite, Adv. Mater. 21 (2009) 2463–2485, https://doi.org/10.1002/adma.200802849.
- [32] D. Treves, Studies on orthoferrites at the Weizmann Institute of Science, J. Appl. Phys. 36 (1965) 1033–1039, https://doi.org/10.1063/1.1714088.
- [33] A.I. Ruiz, M.a.L. López, C. Pico, M.a.L. Veiga, New La_{2/3}TiO₃ derivatives: structure and impedance spectroscopy, J. Solid State Chem. 163 (2002) 472–478, https://doi.org/10.1006/jssc.2001.9430.
- [34] S.M. Lawson, G. Greaves, L.R. Blackburn, R. Chapman, N.C. Hyatt, C.L. Corkhill, Synthesis and in situ ion irradiation of A-site deficient zirconate perovskite ceramics, J. Mater. Chem. A 8 (2020) 19454, https://doi.org/10.1039/ D0TA05255H.
- [35] F. Bahri, A. Simon, H. Khemakhem, J. Ravez, Classical or relaxor ferroelectric behaviour of ceramics with composition Ba_{1-x}Bi_{2x/3}TiO₃, Phys. Stat. Sol. 184 (2001) 459–464, https://doi.org/10.1002/1521-396X(200104)184.
- [36] I. Ueda, S. Ikegami, Piezoelectric properties of modified PbTiO₃ ceramics, Jpn. J. Appl. Phys. 7 (1968) 236. https://iopscience.iop.org/article/10.1143/JJAP.7.236.
 [37] R. Cohen, Ferroelectricity revisited—advances in materials and physics, Nature
- [37] R. Cohen, Ferroelectricity revisited—advances in materials and physics, Nature 359 (2000) 239–458, https://doi.org/10.1016/S0081-1947(01)80020-5.
- [38] A. Huq, M. Kirkham, P.F. Peterson, J.P. Hodges, P.S. Whitfield, K. Page, T. Hügle, E.B. Iverson, A. Parizzi, G. Rennich, POWGEN: rebuild of a third-generation powder diffractometer at the Spallation Neutron Source, J. Appl. Cryst. 52 (2019) 1189–1201, https://doi.org/10.1107/s160057671901121x.
- [39] V. Siruguri, P. Babu, M. Gupta, A. Pimpale, P. Goyal, A high resolution powder diffractometer using focusing optics, Pramana 71 (2008) 1197–1202, https://doi. org/10.1007/s12043-008-0246-2.
- [40] T. Roisnel, J. Rodríquez-Carvajal, WinPLOTR: A Windows Tool for Powder Diffraction Pattern Analysis, Materials Science Forum, Transtec Publications, 1999, 2001, p. 118.
- [41] A. Coelho, Whole-profile structure solution from powder diffraction data using simulated annealing, J. Appl. Cryst. 33 (2000) 899–908, https://doi.org/10.1107/ S002188980000248X.
- [42] K. Nagamalleswari, P. Tulasirao, P. Mandal, A measurement setup for characterization of temperature dependence of impedance, dielectric permittivity, and pyroelectric current under a controlled environment, J. Electron. Mater. 52 (2023) 1625–1632, https://doi.org/10.1007/s11664-022-09875-2.
- [43] K.M. Ok, E.O. Chi, P.S. Halasyamani, Bulk characterization methods for non-centrosymmetric materials: second-harmonic generation, piezoelectricity, pyroelectricity, and ferroelectricity, Chem. Soc. Rev. 35 (2006) 710–717, https://doi.org/10.1039/B511119F.
- [44] Q.Q. Wang, Z. Wang, X.Q. Liu, X.M. Chen, Improved structure stability and multiferroic characteristics in CaTiO₃-modified BiFeO₃ ceramics, J. Am. Ceram. Soc. 95 (2012) 670–675, https://doi.org/10.1111/j.1551-2916.2011.04824.x.
- [45] R. Guo, L. Cross, S. Park, B. Noheda, D. Cox, G. Shirane, Origin of the high piezoelectric response in PbZr_{1-x}Ti_xO₃, Phys. Rev. Lett. 84 (2000) 5423–5426, https://doi.org/10.1103/PhysRevLett.84.5423.
- [46] B. Ruette, S. Zvyagin, A.P. Pyatakov, A. Bush, J. Li, V. Belotelov, A. Zvezdin, D. Viehland, Magnetic-field-induced phase transition in BiFeO₃ observed by high-field electron spin resonance: cycloidal to homogeneous spin order, Phys. Rev. B 69 (2004), 064114, https://doi.org/10.1103/PhysRevB.69.064114.
- [47] H. Feng, The role of Coulomb and exchange interaction on the Dzyaloshinskii-Moriya interaction (DMI) in BiFeO₃, J. Magn. Magn. Mater. 322 (2010) 1765–1769, https://doi.org/10.1016/j.jmmm.2009.12.025.
- [48] V. Khomchenko, L. Pereira, J. Paixão, Weak ferromagnetism and nanodimensional ferroelectric domain structure stabilized in the polar phase of $Bi_{1-x}Nd_xFeO_3$ multiferroics via Ti doping, J. Appl. Phys. 115 (2014), 164101, https://doi.org/10.1063/1.4873121.
- [49] S. Li, W. Cao, L. Cross, The extrinsic nature of nonlinear behavior observed in lead zirconate titanate ferroelectric ceramic, J. Appl. Phys. 69 (1991) 7219–7224, https://doi.org/10.1063/1.347616.
- [50] J.T.S. Irvine, D.C. Sinclair, A.R. West, Electroceramics: characterization by impedance spectroscopy, Adv. Mater. 2 (1990) 132, https://doi.org/10.1002/ adma.19900020304.
- [51] J. Kolte, P.H. Salame, A. Daryapurkar, P. Gopalan, Impedance and AC conductivity study of nano crystalline, fine grained multiferroic bismuth ferrite (BiFeO₃),

synthesized by microwave sintering, AIP Adv. 5 (2015), 097164, <code>https://doi.org/10.1063/1.4931818</code>.